Photoacoustics 38 (2024) 100615

Contents lists available at ScienceDirect

Photoacoustics

journal homepage: www.elsevier.com/locate/pacs

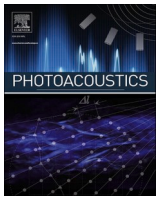

Multimodal PA/US imaging in Rheumatoid Arthritis: Enhanced correlation with clinical scores

Zhibin Huang [a,1], Dongzhou Liu [b,1], Sijie Mo [a,1], Xiaoping Hong [b], Jingyi Xie [b], Yulan Chen [b], Lixiong Liu [b], Di Song [a], Shuzhen Tang [a], Huaiyu Wu [a,*], Jinfeng Xu [a,*], Fajin Dong [a,*]

[a] Department of Ultrasound, The Second Clinical Medical College, Jinan University (Shenzhen People's Hospital), Shenzhen 518020, China
[b] Department of Rheumatology and Immunology, The Second Clinical Medical College, Jinan University (Shenzhen People's Hospital), Shenzhen 518020, China

ARTICLE INFO

Keywords:
Rheumatoid Arthritis
Photoacoustic Imaging
Oxygen Saturation
Ultrasound
Clinical Research

ABSTRACT

Background: Accurate assessment of Rheumatoid Arthritis (RA) activity remains a challenge. Multimodal photoacoustic/ultrasound (PA/US) joint imaging emerges as a novel imaging modality capable of depicting microvascularization and oxygenation levels in inflamed joints associated with RA. However, the scarcity of large-scale studies limits the exploration of correlating joint oxygenation status with disease activity.

Objective: This study aimed to explore the correlation between multimodal PA/US imaging scores and RA disease activity, assessing its clinical applicability in managing RA.

Methods: In this study, we recruited 111 patients diagnosed with RA and conducted examinations of seven small joints on their clinically dominant side using a PA/US imaging system. The PA and power Doppler ultrasound (PDUS) signals were semi-quantitatively assessed using a 0–3 grading system. The cumulative scores for PA and PDUS across these seven joints (PA-sum and PDUS-sum) were calculated. Relative oxygen saturation (So_2) values of inflamed joints on the clinically dominant side were measured, and categorized into four distinct PA+So_2 patterns. The correlation between PA/US imaging scores and disease activity indices was systematically evaluated.

Results: Analysis of 777 small joints in 111 patients revealed that the PA-sum scores exhibited a strong positive correlation with standard clinical scores for RA, including DAS28 [ESR] ($\rho = 0.682$), DAS28 [CRP] ($\rho = 0.683$), CDAI ($\rho = 0.738$), and SDAI ($\rho = 0.739$), all with $p < 0.001$. These correlations were superior to those of the PDUS-sum scores (DAS28 [ESR] $\rho = 0.559$, DAS28 [CRP] $\rho = 0.555$, CDAI $\rho = 0.575$, SDAI $\rho = 0.581$, $p < 0.001$). Significantly, in patients with higher PA-sum scores, notable differences were observed in the erythrocyte sedimentation rate (ESR) ($p < 0.01$) and swollen joint count 28 (SJC28) ($p < 0.01$) between hypoxia and intermediate groups. Notably, RA patients in the hypoxia group exhibited higher clinical scores in certain clinical indices.

Conclusion: Multi-modal PA/US imaging introduces potential advancements in RA assessment, especially regarding So_2 evaluations in synovial tissues and associated PA scores. However, further studies are warranted, particularly with more substantial sample sizes and in multi-center settings.

Summary: This study utilized multi-modal PA/US imaging to analyze Rheumatoid Arthritis (RA) patients' synovial tissues and affected joints. When juxtaposed with traditional PDUS imaging, the PA approach demonstrated enhanced sensitivity, especially concerning detecting small vessels in thickened synovium and inflamed tendon sheaths. Furthermore, correlations between the derived PA scores, PA+So_2 patterns, and standard clinical RA scores were observed. These findings suggest that multi-modal PA/US imaging could be a valuable tool in the comprehensive assessment of RA, offering insights not only into disease activity but also into the oxygenation

Abbreviations: RA, rheumatoid arthritis; PA, photoacoustic; US, ultrasound; PDUS, power Doppler ultrasound; EULAR/ACR, European and American College of Rheumatology; PA/US, Photoacoustic/ultrasound; So_2, oxygen saturation; MRI, magnetic resonance imaging; CDAI, clinical disease activity index; CRP, C-reactive protein; DAS28, 28-joint disease activity score; EGA, evaluator global assessment; ESR, erythrocyte sedimentation rate; PGA, patient global assessment; SDAI, simplified disease activity index; SJC, swollen joint count; TJC, tender joint count; PainVAS, pain visual analog scale; MS, morning stiffness; HAQ, health assessment questionnaire; IQR, interquartile range; 95%CI, 95% confidence interval.

* Corresponding authors.
E-mail addresses: wuhuaiyuszhospital@gmail.com (H. Wu), xujinfeng@yahoo.com (J. Xu), dongfajin@szhospital.com (F. Dong).

[1] These authors contributed equally to this work.

https://doi.org/10.1016/j.pacs.2024.100615
Received 5 February 2024; Received in revised form 25 April 2024; Accepted 5 May 2024
Available online 13 May 2024

status of synovial tissues. However, as promising as these results are, further investigations, especially in larger and diverse patient populations, are imperative.

Key points: ↓ Multi-modal PA/US Imaging in RA: This novel technique was used to assess the So_2 values in synovial tissues and determine PA scores of affected RA joints.

↓ Correlation significantly with Clinical RA Scores: Correlations significantly were noted between PA scores, PA+So_2 patterns, and standard clinical RA metrics, hinting at the potential clinical applicability of the technique.

1. Introduction

Rheumatoid arthritis (RA) is a chronic autoimmune disorder characterized by symmetrical inflammation of synovial joints. Repeated episodes of joint inflammation can culminate in irreversible structural deterioration and functional impairment of the affected joints [1]. Presently, the consensus treatment objectives for RA encompass achieving either complete remission (CR) or low disease activity (LDA) [2]. Nonetheless, a subset of RA patients who attain these therapeutic milestones may still experience relapses in disease activity [3]. This underscores the necessity for more sensitive and objective approaches to monitor synovitis in individuals with RA.

Ultrasound (US) and magnetic resonance imaging (MRI) serve as prevalent non-invasive imaging modalities for the assessment of arthritis [4]. Particularly in the context of rheumatoid arthritis (RA), US has garnered increasing attention owing to its cost-effectiveness and the utility of high-frequency grayscale ultrasound probes. While extant literature substantiates the instrumental role of US in the optimized management of RA [5], discordant findings have been reported, thereby raising questions about the reliability of US for RA evaluation [6]. Specifically, some studies have posited that US can effectively predict relapse in RA patients following medication tapering [7], whereas others have contested its applicability for disease management [8,9]. Moreover, the sensitivity of power Doppler ultrasound (PDUS) in detecting microvascular inflammation has been called into question [10].

Microvascularity plays a pivotal role in the pathogenesis of RA, with neovascularization being a hallmark of synovial inflammation [11–13]. This neovascularization supports the inflamed synovium, contributing to the persistence of inflammation and joint damage. Despite the current recognition of PDUS as the gold standard [14–17] for detecting active inflammation in joints with swelling or tenderness, its resolution limitations hinder its effectiveness in accurately capturing the complex and subtle changes within the inflamed synovial microvasculature [18–20]. Although PDUS demonstrates good sensitivity for low-velocity blood flow, it still faces limitations regarding the detection of slow flow and flow within the small vessels of neo-angiogenesis [21–24]. Given these considerations, there is an imperative need to innovate diagnostic adjuncts that augment the performance of US in the assessment of RA.

Tissue hypoxia, marked by diminished oxygen tension within the tissue, stands as a prominent characteristic of inflammatory pathologies, notably RA [25,26]. The inflammatory response signaling pathway precipitated by hypoxia also represents a therapeutic target in RA management [26]. Consequently, the detection of tissue hypoxia can furnish insights into disease activity and guide individualized therapeutic regimens for RA. While existing research has corroborated the manifestation of hypoxia in RA synovitis [27–29], in vivo delineation of synovial hypoxia and discernment of its role in RA continue to pose challenges.

Photoacoustic (PA) imaging, an innovative medical imaging modality rooted in laser-induced ultrasound, boasts extensive clinical utility for the detection of a diverse range of diseases [30–36]. Through the quantification of signals from oxygenated and deoxygenated hemoglobin in dual-wavelength PA imaging, it holds promise for evaluating the oxygenation status in RA patients [37]. Concurrently, by gauging the hemoglobin concentration in localized tissues, PA imaging can delineate microvascular structures within the synovium of joints afflicted by RA. Of significance is the capacity of PA imaging to seamlessly integrate with conventional ultrasound apparatus, culminating in dual-modality PA-US imaging, thus fostering its clinical translational potential [38]. While several investigations have employed PA imaging to appraise arthritis in RA patients [39–41], these studies have often been constrained by limited sample sizes. Moreover, scant research has holistically juxtaposed oxygenation metrics derived from PA imaging and PA scores against established clinical assessment techniques in RA. To truly harness the clinical implications and utility of PA imaging in rheumatoid arthritis, there is a pressing need for expanded studies centered on its clinical validation and evaluation.

In the present study, we employed a multimodal PA/US imaging system to image the joints of RA patients, aiming to evaluate inflammatory activity across an expanded cohort of participants. Our objectives were twofold: First, to discern the correlation between multimodal PA/US imaging scores and lesion-specific relative oxygen saturation (So_2) values in the context of various RA disease activity indices; And second, given the concerns about the reliability of US for RA evaluation, our study also seeks to quantify intra- and interobserver variability as a secondary aim. This is crucial for establishing PA/US imaging as reliable tools for RA assessment.

2. Materials and methods

The imaging system was developed through a collaborative effort with Mindray Biomedical Electronics. This research was conducted as a retrospective study. All experimental protocols were sanctioned by the Institutional Review Board of Shenzhen People's Hospital (Approval Number: SYL-202161–02). In accordance with ethical guidelines, written informed consent was duly procured from all enrolled patients.

2.1. Participants

From 2022–2023, two expert rheumatologists sequentially enrolled patients with RA from rheumatology outpatient clinics. These patients were diagnosed in accordance with the 2010 European and American College of Rheumatology (EULAR/ACR) criteria [42]. The following represents the exclusion criteria for this study:

Exclusion Criteria: a. Presence of skin damage, open wounds, or ulcers within the imaging area. b. Manifestations such as subcutaneous hyperemia, hemorrhagic purpura, melanoma, port-wine stain, prominent tattoos, or extensive black hair coverage in the imaging area. c. Individuals with a history of psychiatric disorders currently deemed non-cooperative. d. Light-sensitive skin or severe skin conditions, including psoriasis. and e. mixed connective tissue disease.

2.2. Multimodal PA/US imaging system

We employed a commercial US device from Mindray Biomedical Electronics, augmented with an adaptive optical parametric oscillator laser sourced from InnoLas Laser. The imaging was facilitated by a handheld linear PA/US L9–3 probe (for intricate settings and device, please consult Appendix E1). A one-two bifurcated optical fiber bundle (Ceramoptec GmbH), which was mounted by a custom-made holder onto the both sides of the probe, was used to deliver the laser. The laser was emitted to tissues while the generated photoacoustic signals, which presented as the form of ultrasonic waves, were detected by the linear

ultrasonic transducer. An OPO tunable laser (Spitlight 600-OPO, Innolas laser GmbH), which generated 680–980 nm laser pulses at 10 Hz, were utilized. In this study, 750 nm and 830 nm wavelengths were selected for PA imaging, at which the deoxygenated hemoglobin and oxygenated hemoglobin could reach the peak absorption respectively. The ultrasound and photoacoustic signals acquired by the transducer are subjected to preprocessing steps such as amplification and filtering. The image reconstruction for both signals employ the conventional Delay and Sum Beamforming technique. The reconstructed ultrasound and photoacoustic images are then fused through post-processing into a single dual-modality ultrasound/photoacoustic image.

In the multimodal mode, the real-time imaging screen was divided into four segments. The top-left quadrant presented a standard US image, permitting the selection of grayscale ultrasound (GSUS), color Doppler US, or PDUS. The bottom two quadrants displayed photoacoustic images superimposed on GSUS images at wavelengths of 750 nm and 830 nm, respectively. The top-right quadrant showcased So_2 mapping in pseudocolor, representing oxygenation derived from the combined signals of the two photoacoustic images at 750 nm and 830 nm. This system is programmed to autonomously calculate So_2 values, capitalizing on an embedded algorithm (for comprehensive formulae and validation of So_2 computations, refer to document [43]).

2.3. Ultrasound examination and interpretation imaging options

Our selection of joints for the multimodal PA/US evaluation was informed by the seven-joint ultrasound scoring system (US7) proposed by Backhaus et al. [44,45]. We focused on the dorsal aspects of the clinically predominant side of the second and third metacarpophalangeal joints (MCP2 and MCP3), the second and third proximal interphalangeal joints (PIP2 and PIP3), the second and fifth metatarsophalangeal joints (MTP2 and MTP5), and the wrist. Initial grayscale ultrasound (GSUS) and PDUS imaging were performed on these joints, followed by real-time PA/US imaging. All imaging procedures were conducted by radiologist (HY.MD) with 10 years of experience in musculoskeletal ultrasound and proficient training in system operation.

The imaging procedures were meticulously conducted under controlled environmental conditions with a temperature range of 20–25℃ and humidity maintained between 50% and 70%. Prior to the examination, laser safety glasses were provided to both the operator and the patients to ensure compliance with safety protocols. The probe, positioned on the gel pad, was meticulously aligned to ensure that the largest sagittal-sectional view of the lesion (marked by pronounced synovial proliferation and blood flow) was centralized on the display screen. Once the photoacoustic mode is activated and the shutter flash is initiated, the laser emitter begins to operate. We wait approximately 3 seconds to ensure the energy from the laser emitter stabilizes before starting to observe and record the photoacoustic images. By storing about 3 seconds of video, we finally select a frame within the segment where the photoacoustic signal is stable for further analysis. Additionally, the evaluations of GSUS, PDUS, and PA images were undertaken by a pair of radiologists (JX.MD and FD.MD), each boasting 10 years of expertise in musculoskeletal ultrasonography. Refer to Appendix E2 for details.

2.4. Semi-quantitative PDUS and PA imaging scoring

We adopted the semi-quantitative scoring system introduced by Szkudlarek et al. [46], which designates a PDUS score ranging from 0 to 3, as the benchmark for grading both PDUS and PA images within this research. The scoring system is delineated as follows: Score 0: No blood flow signal within the thickened synovium; Score 1: Sparse, punctate blood flow signals within the thickened synovium; Score 2: Multiple points or band-like blood flow signals covering less than 50% of the proliferative synovial area; Score 3: Abundant blood flow signals covering 50% or more of the thickened synovium area.

We then computed the cumulative scores for PDUS (PDUS-sum, range 0–21) and PA (PA-sum, range 0–21) across the seven joints under investigation for subsequent statistical analyses. Two radiologists (JX.MD and FD.MD), each equipped with 10 years of musculoskeletal US expertise and blinded to the patients' details and clinical presentations of the joints being inspected, independently assessed the images. In the event of scoring disparities, the images were re-evaluated until a unanimous agreement was attained. Refer to Appendix E3 for details.

2.5. Multimodal PA/US measurement of So_2 and PA+So_2 patterns

The radiologist (HY.MD) executed the multimodal PA/US imaging and collated basic demographic information. Following this, another set of radiologists (JX.MD and FD.MD), blind to the participants' specifics, independently assessed the So_2 values within the synovial lining of the targeted joint. Should there arise any disparities in their measurements, the images underwent re-examination until unanimous agreement was achieved. One month later, the initial pair of radiologists (JX.MD and FD.MD) revisited and reassessed So_2 values on the PA images. The study evaluated both the consistency within each observer across the two assessments and the agreement between observers during the first measurement.

The second section of the display, rendered in pseudo-color, was dedicated to the mapping of tissue oxygenation and employed for So_2 measurements. Upon defining the regions of interest (ROIs), the system automatically displayed the relative So_2 value in the screen's lower right quadrant. Each joint's So_2 value was measured twice. Utilizing the K-means clustering method, these So_2 values were categorized into three distinct clusters based on their data distribution (refer to Appendix E4 for specifics). The centroids for these clusters in the feature space were determined to be 69.76%, 81.91%, and 91.02%, respectively. So_2 imaging manifested three pseudo-color combinations: a predominant red signal, a blended color signal, and a chief blue signal. Upon integrating cluster analysis with color differentiation, three oxygenation states emerged:

a. Hyperoxia: Characterized by So_2 values exceeding 86.00% and dominantly red in appearance. b. Intermediate oxidation: With So_2 values ranging between 75.00% and 86.00%, presenting a blend of red and blue hues. c. Hypoxia: Denoted by So_2 values falling below 75.00% and predominantly blue in manifestation.

Following the computation of the So_2 value, we integrated the So_2 value with the PA sum score to formulate a novel metric for RA patients, termed the "PA+So_2 pattern". Patients with a PA sum score of less than 3 were identified as having a negligible PA signal, while those with a score of 3 or higher were perceived as having a pronounced PA signal. Based on the PA sum score and So_2 value, patients were stratified into three categories: Pattren 1, absent or minimal PA signal; Pattren 2, pronounced PA signal accompanied by hyperoxia; Pattern 3 and Pattern 4, pronounced PA signal with intermediate oxygenation and hypoxia, respectively. We further explored the correlations between PA+So_2 models and clinical outcomes. Refer to Appendix E4, Appendix Fig 1, and Appendix Fig 2 for details.

2.6. Clinical evaluation

Clinical data, including age, gender, duration since symptom onset, confirmed disease duration, and duration of morning stiffness (MS), were rigorously documented. Additionally, laboratory parameters such as erythrocyte sedimentation rate (ESR) and C-reactive protein (CRP) were noted. For every patient, detailed assessments were undertaken by two experienced rheumatologists, each with over ten years in the field. These evaluations included the tender joint count (TJC), swollen joint count (SJC), pain visual analog scale (PainVAS; with a scale of 0–10), patient's global activity assessment (PGA), evaluator's global assessment (EGA), health assessment questionnaire (HAQ), the disease

activity score encompassing 28 joints (DAS28), the simplified disease activity index (SDAI), and the clinical disease activity index (CDAI).

2.7. Statistical analysis

Statistical analyses were performed using R 4.2.2 (Copyright (C) 2022 The R Foundation for Statistical Computing). Data following a normal distribution were presented as mean ± SD, while non-normally distributed data were expressed as median with the interquartile range (IQR). Correlations between imaging scores (PDUS-sum score, PA-sum score, and the three PA+So_2 patterns) and clinical metrics were assessed using Spearman's rank correlation coefficient (ρ) [47]. The four PA+So_2 modes (Modes 1, 2, 3, and 4) were regarded as ordinal categorical variables. The strength of the correlation coefficient is categorized as: negligible: $\rho < 0.30$; low: $0.30 < \rho < 0.50$; moderate: $0.50 < \rho < 0.70$; strong: $0.70 < \rho < 0.90$; very strong: $\rho > 0.90$ [48]. The consistency between the two radiologists in terms of interobserver and intraobserver agreement was quantified using the weighted kappa statistic (κ), along with a 95% confidence interval (95% CI). The κ values interpretation is as follows: Poor: $\kappa < 0.20$; Fair: $0.20 < \kappa < 0.40$; Moderate: $0.40 < \kappa < 0.60$; Good: $0.60 < \kappa < 0.80$; Excellent: $0.80 < \kappa < 1.00$ [49].

3. Results

3.1. Characteristics of study participants

We recruited a total of 111 patients with a confirmed diagnosis of RA for the study. Each participant underwent both multimodal PA/US imaging and an exhaustive clinical evaluation. Of these RA patients, there were 25 males and 86 females, with a median age of 56 years (Interquartile Range [IQR]: 45–65 years). Compared to patients without morning stiffness, those with morning stiffness exhibited significantly higher Clinical Disease Activity Index (CDAI) [median: 19, interquartile range (IQR): 13, 30 vs. 12.5, IQR: 7.25, 22; $P < 0.01$], Simplified Disease Activity Index (SDAI) [median: 19.43, IQR: 13.76, 30.1 vs. 12.75, IQR: 6.29, 22.02; $P < 0.01$], DAS28ESR (Disease Activity Score 28 - Erythrocyte Sedimentation Rate) [median: 2.96, IQR: 2.66, 3.31 vs. 2.65, IQR: 1.8, 2.97; $P < 0.01$], DAS28CRP (Disease Activity Score 28 - C-Reactive Protein) [median: 2.96, IQR: 2.66, 3.30 vs. 2.65, IQR: 1.8, 2.96; $P < 0.01$], and higher Pain Visual Analog Scale (PainVAS) [median: 3, IQR: 2, 4 vs. 2, IQR: 2, 3; $P < 0.01$]. No significant differences were observed between patients with and without morning stiffness in terms of PDUS-sum ($P = 0.89$) and PA-sum ($P = 0.05$). Table 1 delineates the specific clinical attributes of the RA patients, categorizing them into two groups: those without morning stiffness and those with morning stiffness.

3.2. Intra- and inter-observer variability

To ascertain the clinical applicability of PA/US imaging in RA management, it is necessary to evaluate the consistency of imaging interpretations. Hence, our study meticulously quantifies intra- and interobserver variability, providing a robust measure of reliability that is essential for the clinical adoption of any imaging modality. In this study, significant intra-observer consistency was observed across multiple imaging modalities. For the PA scores, Reader 1 demonstrated a kappa (κ) coefficient of 0.95 (95% confidence interval: 0.94–0.97), while Reader 2 showed a κ value of 0.95 (95% CI: 0.93–0.97). Within the context of power Doppler ultrasonography (PDUS), Reader 1 had a κ value of 0.93 (95% CI: 0.90–0.95) and Reader 2 yielded a κ of 0.97 (95% CI: 0.95–0.99). Concerning oxygenation status classification, Reader 1 produced a κ of 0.97 (95% CI: 0.95–0.99) and Reader 2 had a κ of 0.98 (95% CI: 0.96–0.99). Moreover, impressive consistency between observers was noted in ultrasonography scoring (PA: $\kappa = 0.92$, 95% CI: 0.89–0.94; PDUS: $\kappa = 0.95$, 95% CI: 0.92–0.97) and in categorizing oxygenation status (PA So_2: $\kappa = 0.95$, 95% CI: 0.93–0.98).

Table 1
Clinical Characteristics of RA Patients Stratified by Presence or Absence of Morning Stiffness Attributed to the Disease.

Variables	Total (n = 111)	NMS (n = 46)	PMS (n = 65)	p
Years†	54.98 ± 13.93	53.41 ± 11.76	56.09 ± 15.28	0.30
Height	159 (155, 165)	158 (153.25, 164.5)	160 (156, 165)	0.13
Weight†	56.55 ± 10.59	55.65 ± 11.31	57.18 ± 10.1	0.46
PDUS-sum	2 (1, 4)	2 (1, 4)	2 (1, 4)	0.89
PA-sum	4 (2, 6)	5 (3, 7.75)	4 (2, 6)	0.05
CRP	11.4 (2.5, 43.18)	8.3 (1.46, 43.02)	15.7 (3.26, 43.16)	0.23
ESR	31 (15, 61.5)	31 (12.75, 66.5)	31 (16, 60)	0.94
TJC28	4 (2, 10)	3 (1, 7.5)	5 (3, 12)	0.02
SJC28	0 (0, 3)	0 (0, 1)	1 (0, 4)	0.02
Onset time (y)	6 (1, 11.5)	7.5 (3, 13)	4 (0.75, 10)	0.10
PGA	5 (3.5, 7)	5 (2, 6)	6 (5, 7)	< 0.01
EGA	5 (4, 6.75)	4.5 (2.25, 6)	6 (5, 7)	< 0.01
HAQ	0.5 (0.12, 1)	0.25 (0, 0.62)	0.62 (0.25, 1.12)	0.01
PainVAS	2 (2, 4)	2 (2, 3)	3 (2, 4)	< 0.01
CDAI	16 (10.5, 26)	12.5 (7.25, 22)	19 (13, 30)	< 0.01
SDAI	16.16 (10.86, 26.36)	12.75 (6.29, 22.02)	19.43 (13.76, 30.1)	< 0.01
DAS28ESR	2.87 (2.41, 3.23)	2.65 (1.8, 2.97)	2.96 (2.66, 3.31)	< 0.01
DAS28CRP	2.87 (2.41, 3.22)	2.65 (1.8, 2.96)	2.96 (2.66, 3.3)	< 0.01

Note. —Except where indicated, data are medians, with IQRs in parentheses. VAS for pain, PGA, and EGA are scored 0–10. DAS28ESR or CRP is determined by the following equation: (0.56 x square (TJC)) + (0.28 x square (SJC)) + (0.7 x natural logarithm (ESR/CRP)) + (0.014 x PGA). SDAI is defined as SJC plus TJC plus EGA plus CRP, and CDAI is defined as SJC plus TJC plus PGA plus EGA. CDAI = clinical disease activity index, CRP =C-reactive protein, DAS28 = 28-joint disease activity score, EGA = evaluator global assessment, ESR = erythrocyte sedimentation rate, PGA = patient global assessment, SDAI = simplified disease activity index, SJC = swollen joint count, TJC =tender joint count, PainVAS = Pain visual analog scale, NMS: absence morning stiffness, PMS: Presence morning stiffness, PA-sum: sum of photoacoustic scores, PDUS-sum: Sum of power doppler ultrasound scores, HAQ = health assessment questionnaire.
†Data are means ± SDs.

3.3. Multimodal imaging scores

In this study, a total of 777 joints with the clinically dominant side across 111 participants underwent evaluation using the PA/US system. The distribution of each PA grade, correlated with the PDUS grade (ranging from 0 to 3), is delineated in Table 2. Of these examined joints,

Table 2
Facet Joint Counts Stratified by PA (Scores 1–3) and Corresponding PDUS Scores.

PDUS score	PA score				Total
	0	1	2	3	
0	381	165	45	4	595
1	13	34	19	4	70
2	8	18	19	6	51
3	4	20	27	10	61
Total	406	237	110	24	777

Note. PA score: photoacoustic scores, PDUS score: power doppler ultrasound scores. The joints with the maximum scores were derived from multiple patients, rather than being limited to 1–2 individuals. Specifically, the 61 joints that received a PDUS score of 3 were sourced from 47 patients with RA, and the 24 joints with a PA score of 3 originated from 18 patients.

10 were concurrently graded at the maximum level for both PA and PDUS. A total of 165 joints received a grade 1 in PA but exhibited no discernible signal on PDUS. Conversely, 25 joints that were graded above 1 on PDUS displayed no signal on PA. Imaging interpretation of PDUS and PA results in Appendix Fig 4.

3.4. Association between PA/PDUS scores and clinical indices of RA disease activity

The relationships between PA-sum scores, PD-sum scores, and RA disease activity indices are detailed in Table 3. The PA-sum demonstrated strong correlations with DAS28ESR ($\rho = 0.682$ [0.541–0.784], $p < 0.0001$), DAS28CRP ($\rho = 0.683$ [0.541–0.800], $p < 0.0001$). These correlations were more robust than those observed with the PDUS-sum (e.g., for DAS28ESR, $\rho = 0.559$ [0.414–0.681], $p = 0.0001$). High positive associations were evident between PA-sum and both CDAI ($\rho = 0.738$ [0.619–0.834], $p < 0.0001$) and SDAI ($\rho = 0.739$ [0.611–0.837], $p < 0.0001$). Thus, PDUS-sum exhibited moderate correlations with CDAI ($\rho = 0.575$ [0.423–0.694], $p < 0.0001$) and SDAI ($\rho = 0.581$ [0.432–0.700], $p < 0.0001$). Furthermore, PA-sum shared a moderate association with PainVAS ($\rho = 0.525$ [0.357–0.664], $p < 0.0001$), whereas PDUS-sum displayed a weaker correlation ($\rho = 0.443$ [0.288–0.576], $p < 0.0001$). Interestingly, neither PA-sum nor PDUS-sum showed correlations with MS or Onset time. Additionally, this study conducted a correlation analysis between PA and PDUS scores of 777 small joints, finding that the correlation between PDUS and PA scores was ρ=0.497 (95%CI: 0.438–0.554), indicating a low positive correlation ($P<0.0001$). Visualization of these associations between PDUS/PA scores and clinical metrics is provided in the Appendix Fig 3 and Table 3. A consistent upward trajectory was noted in each curve, underscoring the congruence between imaging findings and clinical outcomes.

Table 3
Correlation of PDUS/PA-Sum Scores with RA Disease Activity Indicators.

Variable	Methods	Correlation	95% CI	P Value
CRP	PDUS-sum	0.388	0.213–0.544	< 0.0001
	PA-sum	0.336	0.158–0.492	< 0.0004
ESR	PDUS-sum	0.361	0.171–0.520	< 0.0001
	PA-sum	0.322	0.134–0.494	< 0.0006
TJC28	PDUS-sum	0.499	0.329–0.631	< 0.0001
	PA-sum	0.689	0.561–0.776	< 0.0001
SJC28	PDUS-sum	0.457	0.285–0.610	< 0.0001
	PA-sum	0.514	0.346–0.658	< 0.0001
MS (min)	PDUS-sum	0.287	0.104–0.475	< 0.0023
	PA-sum	0.288	0.109–0.460	< 0.0022
Onset time(y)	PDUS-sum	0.104	-0.094–0.280	< 0.2767
	PA-sum	-0.038	-0.230–0.151	< 0.6931
PGA	PDUS-sum	0.515	0.352–0.647	< 0.0001
	PA-sum	0.606	0.445–0.733	< 0.0001
EGA	PDUS-sum	0.495	0.337–0.629	< 0.0001
	PA-sum	0.621	0.473–0.739	< 0.0001
HAQ	PDUS-sum	0.413	0.232–0.560	< 0.0001
	PA-sum	0.459	0.291–0.602	< 0.0001
PainVAS	PDUS-sum	0.443	0.288–0.576	< 0.0001
	PA-sum	0.525	0.357–0.664	< 0.0001
CDAI	PDUS-sum	0.575	0.423–0.694	< 0.0001
	PA-sum	0.738	0.619–0.834	< 0.0001
SDAI	PDUS-sum	0.581	0.432–0.700	< 0.0001
	PA-sum	0.739	0.611–0.837	< 0.0001
DAS28ESR	PDUS-sum	0.559	0.414–0.681	< 0.0001
	PA-sum	0.682	0.541–0.784	< 0.0001
DAS28CRP	PDUS-sum	0.555	0.393–0.680	< 0.0001
	PA-sum	0.683	0.541–0.800	< 0.0001
PDUS-score	PA-score	0.497	0.438–0.554	< 0.0001

Note. VAS for pain, PGA, and EGA are scored 0–10. DAS28ESR or CRP is determined by the following equation: (0.56 x square (TJC)) + (0.28 x square (SJC)) + (0.7 x natural logarithm (ESR/CRP)) + (0.014 x PGA). SDAI is defined as SJC plus TJC plus EGA plus CRP, and CDAI is defined as SJC plus TJC plus PGA plus EGA. CDAI = clinical disease activity index, CRP =C-reactive protein, DAS28 = 28-joint disease activity score, EGA = evaluator global assessment, ESR = erythrocyte sedimentation rate, PGA = patient global assessment, SDAI = simplified disease activity index, SJC = swollen joint count, TJC =tender joint count, PainVAS = Pain visual analog scale, MS =morning stiffness, PA-sum =sum of photoacoustic scores, PDUS-sum =Sum of power doppler ultrasound scores, HAQ = health assessment questionnaire, 95% CI 95% =confidence interval.

3.5. Correlations of PA+So_2 patterns with RA disease activity indices

In our cohort of 111 patients, relative So_2 values were ascertained for all those displaying PA signals. These So_2 values for the small joints ranged from 51.45% to 99.60%. Based on the distribution of relative So_2 values in patients with pronounced PA signals (N=82), we employed the K-means clustering technique to categorize the So_2 values into three distinct clusters. Accordingly, patients were grouped into hyperoxia, intermediate, and hypoxia subgroups. 33 patients exhibited hyperoxia with a relative So_2 value exceeding 86%, 16 were categorized as intermediate (So_2 values between 75% and 86%), and 33 displayed hypoxias with an So_2 value falling below 75% (Refer to Appendix E4, Appendix Fig 1, and Appendix Fig 2 for details). A breakdown of patients by pattern revealed that 29 had minimal PA signals (pattern 1), 33 showed pronounced PA signals with hypoxia (pattern 2), 16 had significant PA signals with intermediate (pattern 3), and 33 manifested evident PA signals accompanied by hyperoxia (pattern 4). The clinical scores corresponding to these four patterns are delineated in Table 4. Statistically significant differences were noted in both ESR ($p < 0.01$) and SJC28 ($p < 0.01$) when contrasting patients with marked PA signals who were categorized as intermediate and hyperoxia (patterns 3 and 4). Additionally, a significant variation in SJC28 ($p < 0.04$) emerged between patients with evident PA signals falling into the hypoxia and hyperoxia categories (patterns 2 and 4). No other metrics showcased significant disparities across the patient groups.

4. Discussion

In this study, we utilized a multimodal PA/US imaging system to assess the facet joints in RA patients across varying disease activities. We examined a total of 777 facet joints from 111 patients. Of these, 82 patients exhibited pronounced photoacoustic signals, while 29 displayed minimal such signals. Delving deeper among the 82 patients: 33 presented with synovial hypoxia, 16 with intermediate synovial oxygenation, and 33 demonstrated synovial hyperoxia. Our findings underscored a significant correlation between PA parameters—namely the PA sum score—and clinical scores. This reaffirms the potential of PA imaging as a viable tool in evaluating RA disease activity. Beyond the conventional grayscale US and PDUS, PA imaging emerges as a novel adjunct to ultrasound systems, offering fresh imaging perspectives that could be instrumental in evaluating RA disease activity.

In our study, we undertook a radiographic evaluation of the small joints in RA patients, encompassing MCP, PIP, MTP, and the wrist, guided by the 0–3 PDUS grading scale and the streamlined US7 scoring system [44,45]. Our study findings indicate that, compared to the PDUS-sum scores, the PA-sum scores of these seven joints demonstrated a significantly enhanced correlation with the standard clinical scores for RA. This indicates that PA imaging offers heightened sensitivity to minor vessels in thickened synovium and inflamed tendon sheaths when compared to PDUS imaging. Notably, lesions with a PDUS score of 3 exhibited pronounced PA signals. In joints with synovial hypertrophy and PDUS scores ranging from 0 to 2, diminished or pronounced photoacoustic signals were observed. This suggests that in certain RA cases, inflammatory activity detectable by PA imaging might elude conventional ultrasound techniques. Furthermore, joints with a PDUS score of 3 were frequently aligned with PA scores of 1 and 2, hinting at the potential of PDUS imaging to overestimate disease activity in RA patients. Our data indicates a mild to moderate association between PDUS scores and clinical scores, with a correlation coefficient spanning 0.36–0.58.

Table 4
Clinical Scores Associated with PA+So_2 Patterns.

Variables	Total (n = 111)	Pattern 1 (n = 29)	Pattern 2 (n = 33)	Pattern 3 (n = 16)	Pattern 4 (n = 33)	p	p§	p‡
CRP	11.4 (2.5, 43.18)	2.68 (0.9, 33.94)	14.5 (4.5, 41.7)	10.85 (2.18, 25.02)	21.06 (5.1, 67.45)	0.02	0.07	0.40
ESR	31 (15, 61.5)	26 (9, 51)	32 (22, 61)	17.5 (13.5, 40.38)	49 (24, 71)	0.03	< 0.01	0.17
TJC28	4 (2, 10)	2 (0, 4)	8 (4, 12)	3 (2, 9.25)	5 (3, 20)	< 0.01	0.14	0.89
SJC28	0 (0, 3)	0 (0, 1)	0 (0, 3)	0 (0, 1.25)	4 (0, 6)	< 0.01	< 0.01	0.04
MS (min)	5 (0, 45)	0 (0, 10)	10 (0, 30)	1 (0, 12.5)	20 (0, 120)	0.06	0.13	0.6
Onset time(y)	6 (1, 11.5)	7 (0.75, 10)	6 (1, 14)	3.5 (1, 15.25)	7 (1, 10)	0.97	0.73	0.72
PGA	5 (3.5, 7)	3 (2, 5)	6 (5, 6)	5.5 (4.5, 6.62)	6 (5, 8)	< 0.01	0.27	0.57
EGA	5 (4, 6.75)	4 (2, 5)	6 (5, 7)	5.5 (4.75, 6)	6 (4, 7)	< 0.01	0.26	0.93
HAQ	0.5 (0.12, 1)	0.12 (0, 0.62)	0.5 (0.25, 1.12)	0.56 (0.09, 0.81)	0.62 (0.25, 1.38)	0.02	0.29	0.94
PainVAS	2 (2, 4)	2 (2, 2)	3 (2, 4)	2.5 (2, 4)	4 (2, 6)	< 0.01	0.4	0.27
CDAI	16 (10.5, 26)	10 (5, 13)	22 (14, 28)	15.5 (11.75, 19.75)	22 (13, 37)	< 0.01	0.10	0.55
SDAI	16.16 (10.86, 26.36)	10.01 (5.01, 13.09)	22.08 (14.98, 29.11)	15.56 (11.76, 20.08)	22.17 (13.39, 37.34)	< 0.01	0.08	0.56
DAS28ESR	2.87 (2.41, 3.23)	2.2 (1.64, 2.7)	3 (2.74, 3.26)	2.91 (2.58, 3.07)	2.98 (2.62, 3.46)	< 0.01	0.18	0.53
DAS28CRP	2.87 (2.41, 3.22)	2.18 (1.64, 2.69)	2.99 (2.72, 3.25)	2.91 (2.58, 3.07)	2.98 (2.62, 3.46)	< 0.01	0.20	0.55

Note. —Except where indicated, data are medians, with IQRs in parentheses. VAS for pain, PGA, and EGA are scored 0–10. DAS28ESR or CRP is determined by the following equation: (0.56 x square (TJC)) + (0.28 x square (SJC)) + (0.7 x natural logarithm (ESR/CRP)) + (0.014 x PGA). SDAI is defined as SJC plus TJC plus EGA plus CRP, and CDAI is defined as SJC plus TJC plus PGA plus EGA. CDAI = clinical disease activity index, CRP =C-reactive protein, DAS28 = 28-joint disease activity score, EGA = evaluator global assessment, ESR = erythrocyte sedimentation rate, PGA = patient global assessment, RA = rheumatoid arthritis, SDAI = simplified disease activity index, SJC = swollen joint count, TJC =tender joint count, PainVAS = Pain visual analog scale, HAQ = health assessment questionnaire. MS= morning stiffness, HAQ = health assessment questionnaire.
Pattern 1: absent or minimal PA signal.
Pattern 2: pronounced PA signal accompanied by hyperoxia.
Pattern 3: pronounced PA signal with intermediate oxygenation.
Pattern 4: pronounced PA signal with hypoxia.
§: Comparison of the hyperoxia and intermediate oxygenation groups.
‡: Comparison of the hyperoxia and hypoxia oxygenation groups.

This is consistent with correlation coefficients ranging from 0.46 to 0.71 reported in prior studies [41,50,51]. When juxtaposed against the PDUS-sum score, the PA-sum score demonstrated a superior correlation coefficient and exhibited a strong positive association with standard clinical disease activity scores ($\rho>0.70$ for both CDAI and SDAI). What's more, the results of our study showed a low positive correlation between PDUS and PA scores ($\rho=0.497$). This result is coherent and interpretable. The PA scoring system was developed as an extension of PDUS scoring [46], designed to enhance sensitivity and specificity in detecting synovial inflammation. The emergence of a low positive correlation between PDUS and PA scores can be attributed to PA scoring's elevated sensitivity and its broader clinical relevance, thus explaining the observed correlation pattern. In summary, PA imaging emerges as a potential tool offering a nuanced reflection of individual patient disease activity, especially in deciphering active lesions that might be overlooked or overstated by PDUS.

The role of hypoxia in RA has been established [25,26]. Fearo et al. also undertook direct measurements of synovial oxygen partial pressure (pO2) in patients with Rheumatoid Arthritis (RA) using arthroscopy and ion-selective electrodes [52]. They identified hypoxic microenvironments within inflamed synovial joints, attributed to the dysregulation and expansion of the microvascular system and the metabolic turnover of the swollen synovium, despite the relatively time-consuming and invasive nature of their methodology. Similarly, in our study, the application of non-invasive PA imaging revealed tissue hypoxia within the thickened synovium of RA participants. Yang et al. indicates that in patients with rheumatoid arthritis, the degree of disease activity is associated with increased synovial hypoxia detected by photoacoustic imaging, even though their research did not incorporate a scoring system for PA imaging [35]. In our study, we employed relative So_2 values identified from PA signal pixels to categorize patients into hyperoxia, intermediate, and hypoxia subtypes. We observed that joints with prominent PA signals in hyperoxia individuals were more likely to have elevated SJC28 compared to hypoxia patients. Furthermore, hyperoxia subjects displayed a higher likelihood of presenting elevated SJC28 and ESR than their intermediate counterparts. The combined PA+So_2 pattern demonstrated a mild positive correlation with SJC28, but no significant association with ESR, suggesting that oxygenation status might relate to the number of swollen joints. The relative So_2 values serve as an adjunct in assessing joint symptoms. No significant differences were noted between the PA+So_2 pattern and PainVAS, PGA, or other indices. These findings are insufficient to delineate the role of oxygenation in gauging disease activity and do not entirely align with Zhao et al.'s research [41]. This discrepancy may arise from uneven case distribution and limited sample size in our study. Future research employing a more balanced and multicentric sample, focusing on oxygenation measurements through PA imaging, is warranted to further validate the utility of dual-wavelength PA in assessing RA.

This study is not without limitations. Firstly, we acknowledge the absence of a gold standard for invasive tissue oxygenation measurements and a secondary standard of MRI for participants. MRI is an important imaging modality in RA and can serve as a reference standard for studying other imaging modalities [53,54] and will be included in future studies. Secondly, our sample of RA patients remains relatively limited, and there's a lack of external validation data. A larger patient cohort and incorporation of multicenter data are essential for further validation. Future studies with expanded sample sizes and multicentric clinical trials are also anticipated to explore the value of So_2 in assessing RA disease activity. Thirdly, our retrospective study, conducted with sequentially enrolled patients by expert rheumatologists and guided by specific inclusion and exclusion criteria, might face selection bias, impacting the generalizability of our findings to the broader RA patient population. Lastly, this research offers a retrospective analysis of the multimodal PA/US imaging system. Whether these PA metrics can predict therapeutic response and the risk of RA relapse remains to be investigated in forthcoming prospective cohort studies. In fact, the inherent subjectivity of this study cannot be completely avoided, and future efforts should explore artificial intelligence and machine learning to enhance imaging analysis. Integrating these directions is expected to broaden the application scope of PA imaging in RA, promoting clinical and technological advancements in the field.

5. Conclusion

We utilized multimodal PA/US imaging to evaluate So_2 in the synovial tissue and PA scores of affected joints in RA patients. The correlations between PA scores, PA+So_2 patterns, and standard clinical RA scores were established. The multimodal PA/US imaging system offers valuable additional imaging parameters and holds substantial potential in assessing disease activity in RA patients.

Funding

This research received no specific grant from any funding agency in the public, commercial, or not-for-profit sectors.

CRediT authorship contribution statement

Fajin Dong: Writing – review & editing, Visualization, Validation, Supervision. **Dongzhou Liu:** Resources, Data curation. **Jingyi Xie:** Formal analysis. **Yulan Chen:** Methodology. **Sijie Mo:** Resources. **Xiaoping Hong:** Data curation. **Shuzhen Tang:** Data curation. **Jinfeng Xu:** Writing – review & editing, Visualization, Supervision. **Lixiong Liu:** Resources. **Di Song:** Resources. **Huaiyu Wu:** Methodology, Formal analysis, Data curation, Conceptualization. **Zhibin Huang:** Writing – original draft, Visualization, Validation, Methodology, Data curation.

Declaration of Competing Interest

The authors declare that they have no known competing financial interests or personal relationships that could have appeared to influence the work reported in this paper.

Data Availability

Data will be made available on request.

Acknowledgments

This work was supported by the Guangdong Basic and Applied Basic Research Foundation (2023A1515220148).

Main author's contribution

Zhibin Huang, the first author, Dongzhou Liu and Sijie Mo, the co-first author, also contributed to this work by conceiving and designing the experiments, analyzing the data, and providing materials/analytical tools. Huaiyu Wu, Jinfeng Xu and Fajin Dong are the corresponding authors and the guarantor of the integrity of the entire study.

Financial support

No.

Appendix E1

Imaging settings and operating procedures of the multimodal PA/US

Imaging system

The multimodal photoacoustic and ultrasound (PA/US) imaging system (Fig E1 and Fig E2) offers horizontal and vertical resolutions under 1 mm, with a signal-to-noise ratio of 27.5 dB within a depth range of 5–20 mm. The system's luminous flux on the tissue surface is less than 20 mJ/cm^2, exhibiting less than a 5% fluctuation. To minimize PA noise, typically observed beneath bone surfaces, the imaging gain value was adjusted from 55 to 45 dB. Power Doppler US (PDUS) imaging parameters included a pulse repetition frequency (PRF) of 600–1000 Hz, a wall filter of 50–100 Hz, a maximum gain of 85–90%, a scale of 3 cm/s, and a rectangular sampling box devoid of angulation.

In the multimodal mode, the real-time imaging screen was divided into four segments. The top-left quadrant presented a standard ultrasound image, permitting the selection of grayscale ultrasound (GSUS), color Doppler US, or Power Doppler US. The bottom two quadrants displayed photoacoustic images superimposed on GSUS images at wavelengths of 750 nm and 830 nm, respectively. The top-right quadrant showcased oxygen saturation (So_2) mapping in pseudocolor, representing oxygenation derived from the combined signals of the two photoacoustic images at 750 nm and 830 nm.

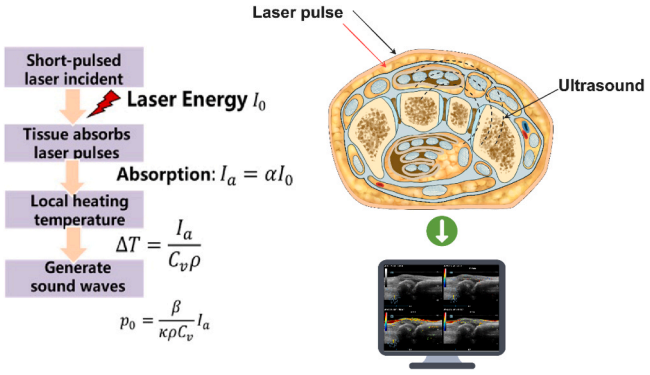

Fig E1. Principles and mechanisms of photoacoustic imaging. Note: This equation "$I_a = \alpha I_0$" describes the energy conversion process from laser energy to acoustic pressure, elucidating how tissue, upon irradiation by a short-pulsed laser with a certain energy (I_0), absorbs part of the laser energy. The amount of absorbed light energy (I_a) is directly proportional to the tissue's absorption coefficient (α), as captured by the equation $I_a = \alpha I_0$.

Following the absorption of light energy, the absorbed energy induces a local temperature rise in the tissue. This temperature increase can be described thermodynamically by the equation $\Delta T = \frac{I_a}{C_v \rho}$, where C_v is the specific heat capacity at constant volume, ρ is the density. According to the thermoelastic effect, the medium undergoes volume expansion and pressure increase. Due to the short-pulsed laser satisfying the constraints of thermal and stress confinements, the relative change in volume expansion can be neglected. This allows for a rapid increase in local pressure, which

propagates in the form of ultrasonic waves. The generated initial sound pressure can be expressed by the equation $p_0 = \frac{\beta}{\kappa \rho C_V} I_a$, where β is the thermal expansion coefficient, κ is the isothermal compressibility, ρ is the density, and C_V is the specific heat capacity at constant volume. The Grueneisen parameter $\Gamma = \frac{\beta}{\kappa \rho C_V}$, is often defined to describe the thermodynamic properties of the tissue, rendering the initial sound pressure as $p_0 = \Gamma I_a$. This initial sound pressure, upon propagation through the medium and detection by an ultrasound transducer, is processed to form a photoacoustic image.

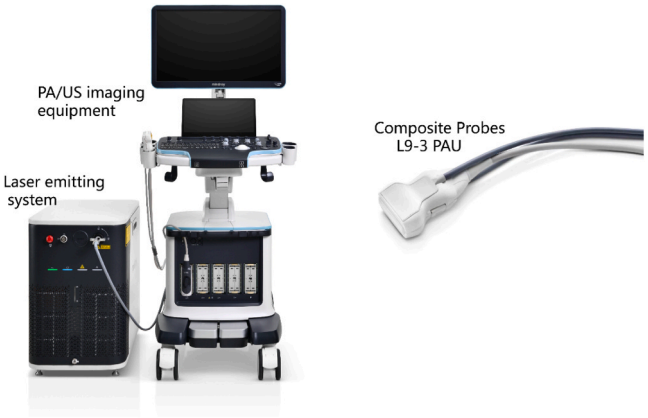

Fig E2. Photoacoustic/ultrasound imaging system and imaging probe (L9–3PAU, center frequency 5.5 MHz).

Appendix E2

Imaging procedures

The imaging studies targeted the following joints: the second metacarpophalangeal joint (MCP2), third metacarpophalangeal joint (MCP3), second proximal interphalangeal joint (PIP2), third proximal interphalangeal joint (PIP3), second metatarsophalangeal joint (MTP2), fifth metatarsophalangeal joint (MTP5), and the clinically dominant side wrist. Imaging was conducted under conditions of 20–25℃ temperature and 50–70% humidity. Prior to the examination, laser safety glasses were provided to both the operator and the patients to ensure compliance with safety protocols. For the procedure, patients were positioned adjacent to the operator with their hands resting on a white surface, positioned beside the imaging apparatus. The ultrasound probe was applied dorsally to the fingers, toes, and wrists in a longitudinal orientation, using an ultrasound gel pad for improved imaging clarity. The probe, positioned on the gel pad, was meticulously aligned to ensure that the largest sagittal-sectional view of the lesion (marked by pronounced synovial proliferation and blood flow) was centralized on the display screen. Specifically, the dorsal sections of the MCP, PIP, and MTP joints were imaged longitudinally. For the wrist joint, landmarks were chosen between the radiocarpal joint and the third metacarpophalangeal joint, with extensor tendons of the hand serving as superficial landmarks. For MCP and PIP joints, the anatomical landmarks were the metacarpal heads/proximal phalangeal bases and proximal phalangeal heads/middle phalangeal bases, respectively, with extensor tendons again serving as superficial landmarks.

The imaging depth was set at 2 cm for the MCP, MTP, and PIP joints, and between 2.5 and 3 cm for the wrist. During PA scanning, the initial section of the display transitioned among various ultrasound modalities, facilitating a comprehensive comparison between US and PA images. Conventional ultrasonography took approximately 30 seconds to 1 minute per joint, while the multimodal PA/US imaging required about 2 minutes. The aggregate examination duration spanned roughly 20–30 minutes. Imaging parameters for both US and PA remained consistent throughout the procedure.

Initial grayscale ultrasonography (GSUS) and power Doppler ultrasonography (PDUS) scans were performed by one operator (HY.MD), with 10 years of musculoskeletal ultrasound expertise and three additional months of training on this specific system. Subsequent real-time photoacoustic and ultrasonic (PA/US) imaging was conducted by the operator. Once the photoacoustic mode is activated and the shutter flash is initiated, the laser emitter begins to operate. We wait approximately 3 seconds to ensure the energy from the laser emitter stabilizes before starting to observe and record the photoacoustic images. By storing about 3 seconds of video, we finally select a frame within the segment where the photoacoustic signal is stable for further analysis.

Appendix E3

The PDUS/PA scoring method

A scoring system ranging from 0 to 3 was employed as follows:

Score 0: Absence of PDUS/PA signals.

Score 1: Minimal PDUS/PA signals (fewer than 3 bars) within inflamed areas, characterized by areas of low echogenicity in hypertrophied synovium, tenosynovitis, or paratenonitis.

Score 2: PDUS/PA signals evident in less than half of the inflamed regions.

Score 3: PDUS/PA signals present in over half of the inflamed regions.

In the initial phase, grayscale ultrasonography (GSUS) was utilized to identify inflammatory lesions, encompassing thickened synovium, hypertrophic tendons, and abnormal hypoechoic areas adjacent to or within the tendon sheaths. These lesions were subsequently classified as either synovitis or tenosynovitis/paratenonitis. Following this, both PDUS and PA imaging of the designated inflammatory sites were semi-quantitatively scored based on the aforementioned system for each joint. For scoring purposes, the initial part of the photoacoustic imaging display was designated for GSUS, while the third and fourth sections, corresponding to Wave1–750 nm and Wave2–830 nm wavelengths, were earmarked for PA scoring.

Additionally, measurement of So_2 at PA Ratio (second part of the screen). Parallelly, PDUS imaging was conducted using a separate but identical device for the PDUS scoring. The highest score (ranging from 0 to 3) obtained for either synovitis or tenosynovitis/paratenonitis determined the conclusive score for each individual joint. The evaluations of GSUS, PDUS, and PA images were undertaken by a pair of radiologists (JX.MD and FD.MD), each boasting 10 years of expertise in musculoskeletal ultrasonography. Importantly, these radiologists (JX.MD and FD.MD) were not privy to patient-specific information or clinical presentations of the joints under examination. In cases where scoring discrepancies arose between the radiologists, the inflamed regions designated for scoring were re-evaluated until a consensus was achieved for each respective joint.

Appendix E4

Relative So_2 values and So_2 sub-grouping

The second section of the display, rendered in pseudo-color, was dedicated to the mapping of tissue oxygenation and employed for So_2 measurements. To distinguish between signals indicative of hyperoxia, intermediate oxygen levels, and hypoxia, integrated signal pixels were quantified to determine relative So_2 values. By comparing the pixel ratios of PA signals in target areas at wavelengths of 750 nm and 830 nm, the relative So_2 of inflamed sites was ascertained. The requisite software, integrated into the ultrasonic system, facilitated this calculation. Radiologists could execute the So_2 computation by delineating target regions on the dedicated interface. Upon defining the regions of interest (ROIs), the system automatically displayed the relative So_2 value in the screen's lower right quadrant. Only joints exhibiting PA signals underwent So_2 calculation, with the joints showcasing the most pronounced PA signals designated as the representative local So_2 values for individual patients. Each joint underwent dual calculations, and the mean of these determinations was deemed representative of a patient's tissue oxygenation status. Each joint's So_2 value was measured twice. Utilizing the K-means clustering method, these So_2 values were categorized into three distinct clusters based on their data distribution (refer to Appendix Fig 1 and Appendix Fig 2 for specifics). The centroids for these clusters in the feature space were determined to be 69.76%, 81.91%, and 91.02%, respectively. So_2 imaging manifested three pseudo-color combinations: a predominant red signal, a blended color signal, and a chief blue signal. Upon integrating cluster analysis with color differentiation, three oxygenation states emerged:

a. Hyperoxia: Characterized by So_2 values exceeding 86.00% and dominantly red in appearance. b. Intermediate oxidation: With So_2 values ranging between 75.00% and 86.00%, presenting a blend of red and blue hues. c. Hypoxia: Denoted by So_2 values falling below 75.00% and predominantly blue in manifestation.

Appendix

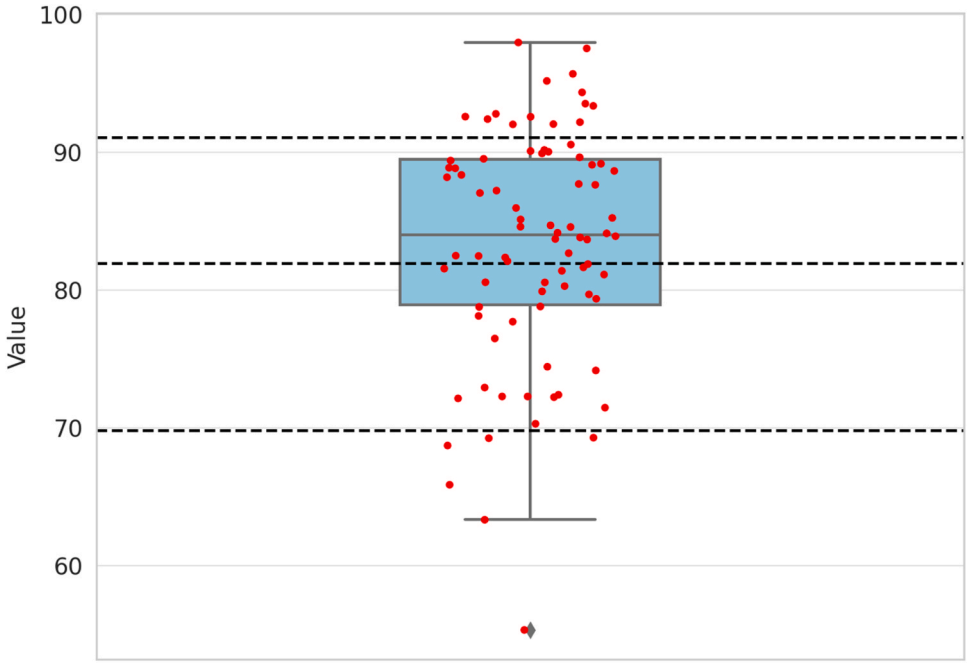

Fig 1. Note: Box plots of the relative So_2 values of the 82 RA patients (PA sum $\geq$3) allowed the observation of a triple distribution of the 82 values.

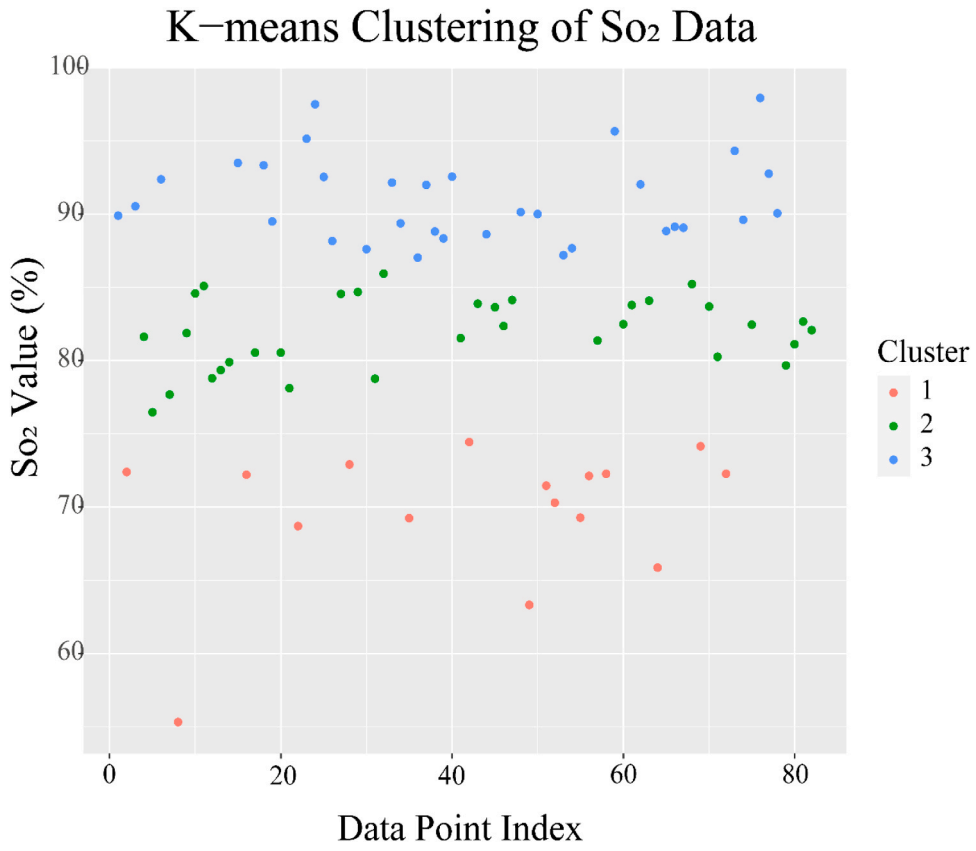

Fig 2. : Cluster analysis on So_2. Note: Cluster plots of the relative So_2 values of the 82 RA patients (PA sum ≥3) allowed the observation of a triple distribution of the 82 values.

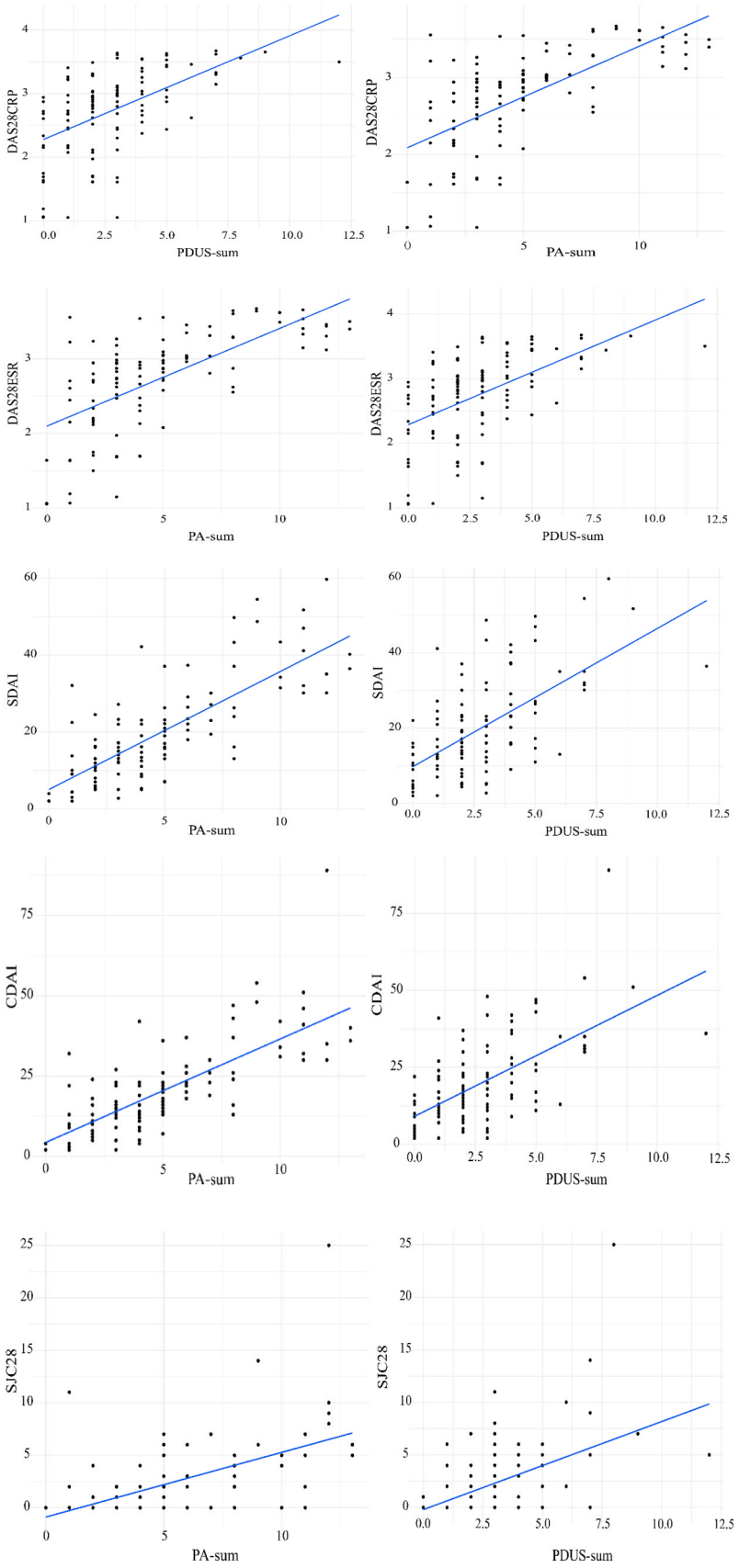

Fig 3. Correlation Curves of PDUS-sum/PA-sum Scores with Clinical Metrics.

Appendix Fig 4:

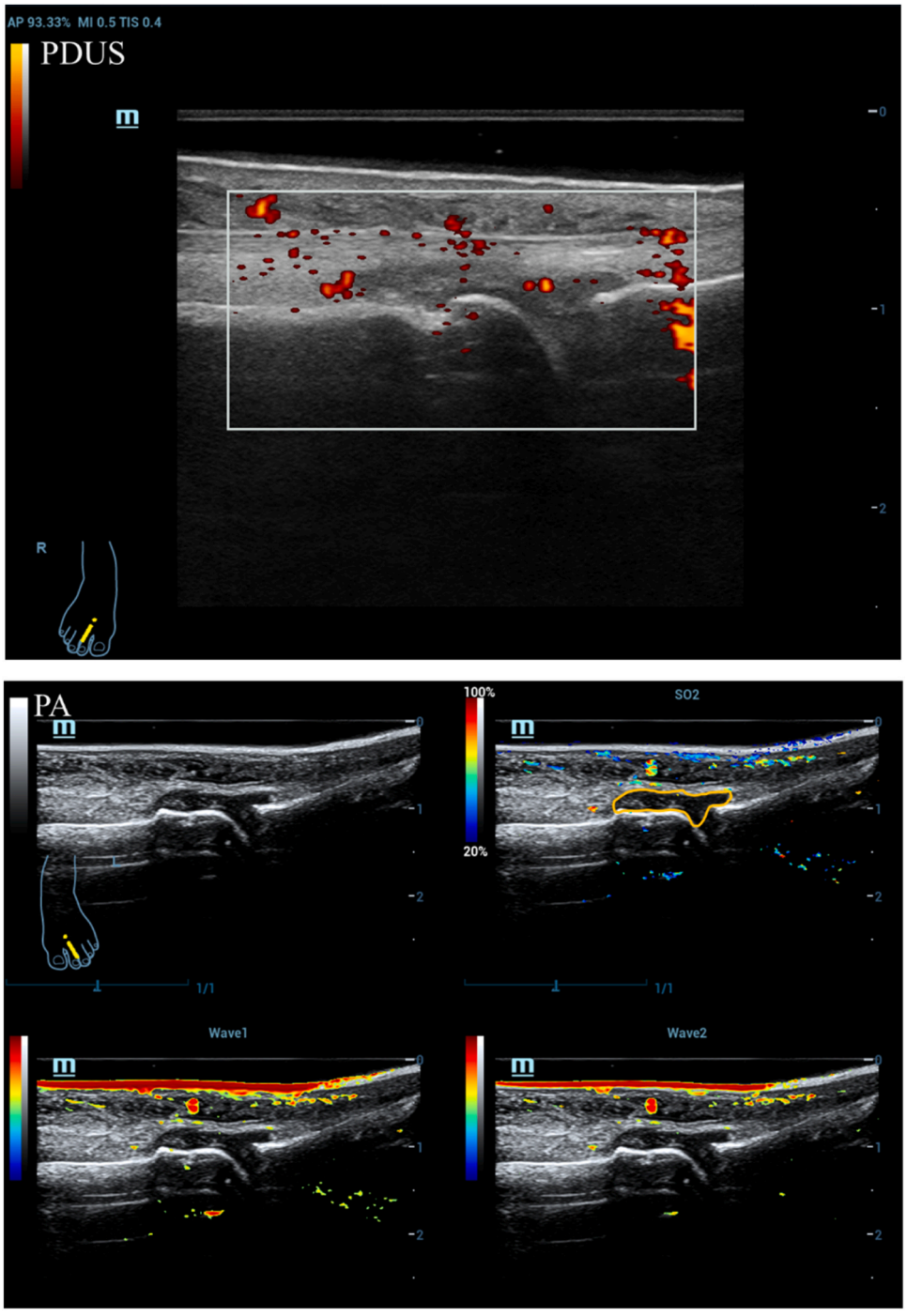

Example 1. PDUS0, PA 1 (PA: photoacoustic imaging; PDUS: power Doppler US).

Patient Profile: 40-year-old woman with a 1-year history of RA. Site: Dorsal aspect of MTP2. GSUS: Located at "PA screen upper left corner"; PA Imaging: 750 nm at 'PA screen lower left corner', 830 nm at "PA screen lower right corner". So_2 Imaging: Located at "PA screen upper right corner", showing a blue pseudo-color signal, indicative of a relative So_2 value of 69.00%, which is categorized as hypoxia. Observation: No significant PDUS signal detected in the thickened synovium of MTP2 (scored as 0). PA signals at 830 nm wavelength showed signal within the hypoechoic region. PA signals in the skin layer resulted from melanin light absorption.

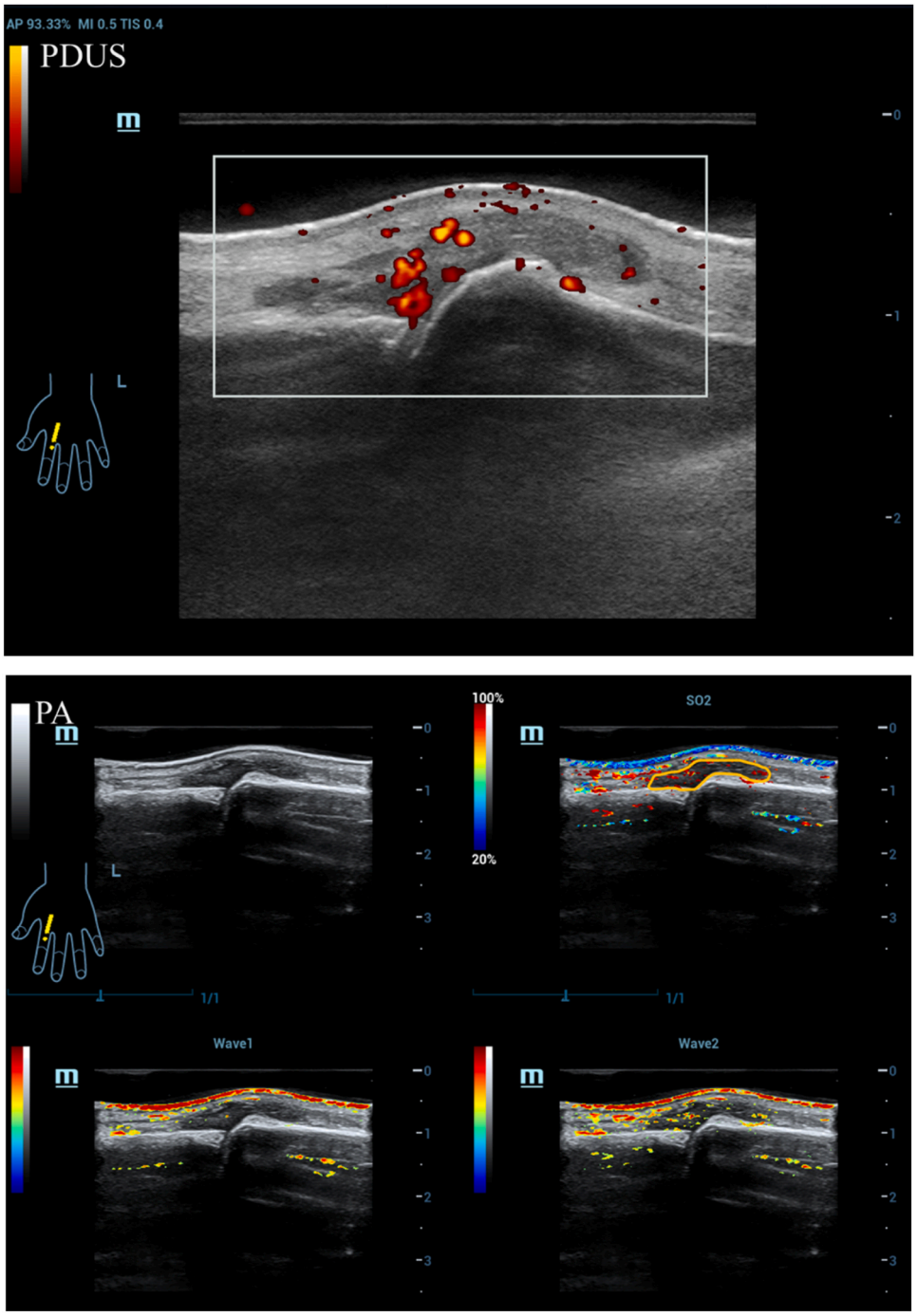

Example 2. PDUS2, PA 3.

Patient Profile: 37-year-old woman with a 1-month history of RA. Site: Dorsal aspect of MCP2. Observation: In PDUS mode, a significant signal is presented (scored 2). Abundant PA signals at both wavelengths indicate congestion of the inflamed lesion. The PA score for MCP2 is 3. In the So_2 section, signals show in red pseudo-color, with a relative So_2 value of 94.94%, classified as hyperoxia.

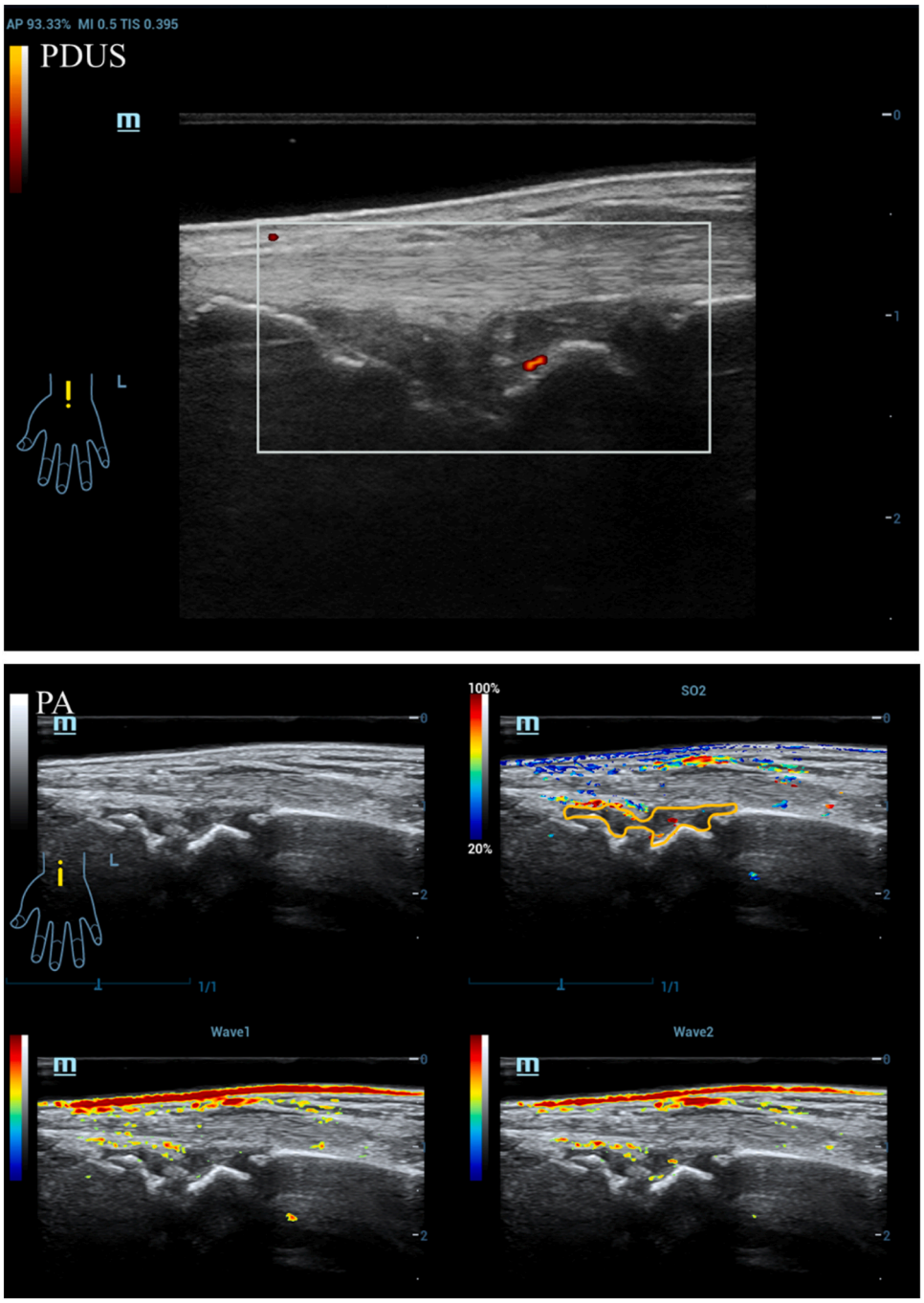

Example 3. PDUS 1, PA 2

Patient Profile: 60-year-old woman with a 2-year history of RA. Site: Dorsal aspect of Wrist. Observation: The synovium is notably thickened, with an area of hypoxia detected above the hyperechoic line of Wrist. Few vessels detected at the lesion margins in PDUS, scoring it 1. PA signals are distributed across two wavelengths. So_2 signals are a mix of red and blue, with a relative So_2 value of 84.18%, categorized as intermediate oxygenation.

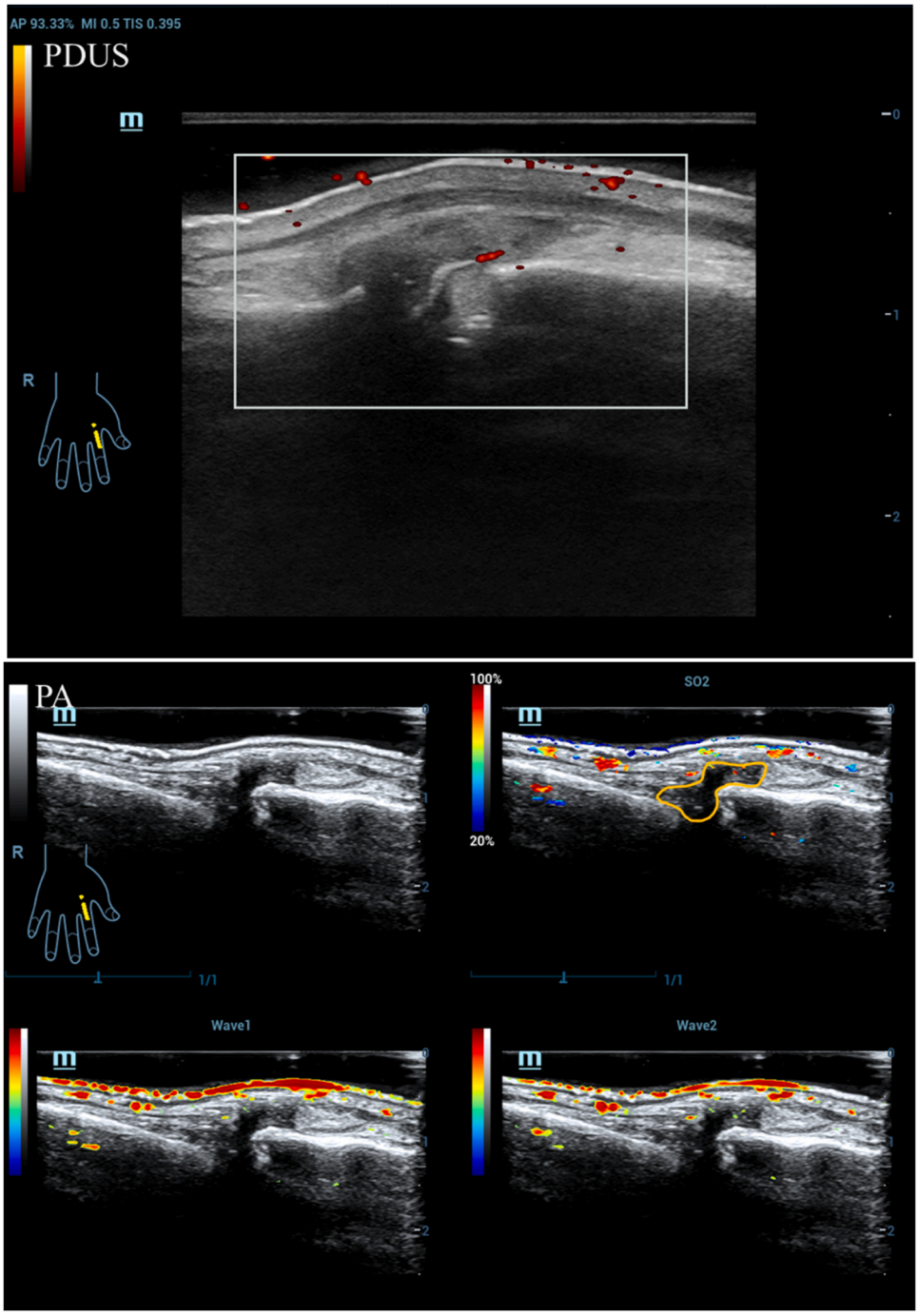

Example 4. PDUS1, PA1

Patient Profile: 59-year-old woman with a 1.5-year history of RA. Site: Dorsal aspect of MCP2. Observation: A notably thickened synovium shows an area of hypoxia above the hyperechoic line of MCP2. Few vessels are detected at the lesion margins in PDUS, scoring it 1. PA images at 830 nm wavelength display several signals. In the So2 section, signals are blue pseudo-colored, with a relative So2 value of 77.43%, classified as intermediate oxygenation.

References

[1] F. Matcham, I.C. Scott, L. Rayner, M. Hotopf, G.H. Kingsley, S. Norton, D.L. Scott, S. Steer, The impact of rheumatoid arthritis on quality-of-life assessed using the SF-36: a systematic review and meta-analysis, Semin. Arthritis Rheumatism 44 (2) (2014) 123–130.

[2] J.S. Smolen, F.C. Breedveld, G.R. Burmester, V. Bykerk, M. Dougados, P. Emery, T. K. Kvien, M.V. Navarro-Compán, S. Oliver, M. Schoels, Treating rheumatoid arthritis to target: 2014 update of the recommendations of an international task force, Ann. Rheumatic Dis. 75 (1) (2016) 3–15.

[3] T. Kuijper, J. Luime, P. De Jong, A. Gerards, D. van Zeben, I. Tchetverikov, P. de Sonnaville, M. van Krugten, B. Grillet, J. Hazes, Tapering conventional synthetic DMARDs in patients with early arthritis in sustained remission: 2-year follow-up of the tREACH trial, Ann. RHEUMATIC Dis. 75 (12) (2016) 2119–2123.

[4] A.N. Colebatch, C.J. Edwards, M. Østergaard, D. van der Heijde, P.V. Balint, M.-A. D'Agostino, K. Forslind, W. Grassi, E.A. Haavardsholm, G. Haugeberg, EULAR

recommendations for the use of imaging of the joints in the clinical management of rheumatoid arthritis, Ann. Rheumatic Dis. 72 (6) (2013) 804–814.
[5] C. Ciurtin, A. Jones, G. Brown, F.E. Sin, C. Raine, J. Manson, I. Giles, Real benefits of ultrasound evaluation of hand and foot synovitis for better characterisation of the disease activity in rheumatoid arthritis, Eur. Radiol. 29 (2019) 6345–6354.
[6] R. Caporali, J.S. Smolen, Back to the future: forget ultrasound and focus on clinical assessment in rheumatoid arthritis management, Ann. Rheumatic Dis. 77 (1) (2018) 18–20.
[7] E. Naredo, L. Valor, I. De la Torre, M. Montoro, N. Bello, J. Martínez-Barrio, L. Martínez-Estupiñán, J.C. Nieto, J.G. Ovalles-Bonilla, D. Hernández-Flórez, et al., Predictive value of Doppler ultrasound-detected synovitis in relation to failed tapering of biologic therapy in patients with rheumatoid arthritis, Rheumatology 54 (8) (2015) 1408–1414.
[8] E.A. Haavardsholm, A.-B. Aga, I.C. Olsen, S. Lillegraven, H.B. Hammer, T. Uhlig, H. Fremstad, T.M. Madland, Å.S. Lexberg, H. Haukeland, et al., Ultrasound in management of rheumatoid arthritis: ARCTIC randomised controlled strategy trial, BMJ (Clin. Res. Ed.) 354 (2016) i4205.
[9] J. Dale, A. Stirling, R. Zhang, D. Purves, J. Foley, M. Sambrook, P.G. Conaghan, D. van der Heijde, A. McConnachie, I.B. McInnes, et al., Targeting ultrasound remission in early rheumatoid arthritis: the results of the TaSER study, a randomised clinical trial, Ann. Rheumatic Dis. 75 (6) (2016) 1043–1050.
[10] H. Nguyen, A. Ruyssen-Witrand, F. Gandjbakhch, A. Constantin, V. Foltz, A. Cantagrel, Prevalence of ultrasound-detected residual synovitis and risk of relapse and structural progression in rheumatoid arthritis patients in clinical remission: a systematic review and meta-analysis, Rheumatology 53 (11) (2014) 2110–2118.
[11] U. Fearon, M. Canavan, M. Biniecka, D.J. Veale, Hypoxia, mitochondrial dysfunction and synovial invasiveness in rheumatoid arthritis, Nat. Rev. Rheumatol. 12 (7) (2016) 385–397.
[12] D.J. Veale, C. Orr, U. Fearon, Cellular and molecular perspectives in rheumatoid arthritis, Semin. Immunopathol. 39 (4) (2017) 343–354.
[13] H.A. Elshabrawy, Z. Chen, M.V. Volin, S. Ravella, S. Virupannavar, S. Shahrara, The pathogenic role of angiogenesis in rheumatoid arthritis, Angiogenesis 18 (4) (2015) 433–448.
[14] A.Y. Park, B.K. Seo, S.H. Cha, S.K. Yeom, S.W. Lee, H.H. Chung, An innovative ultrasound technique for evaluation of tumor vascularity in breast cancers: superb micro-vascular imaging, J. Breast Cancer 19 (2) (2016) 210.
[15] J.M. Koski, S. Saarakkala, M. Helle, U. Hakulinen, J.O. Heikkinen, H. Hermunen, Power Doppler ultrasonography and synovitis: correlating ultrasound imaging with histopathological findings and evaluating the performance of ultrasound equipments, Ann. RHEUMATIC Dis. 65 (12) (2006) 1590–1595.
[16] J. Rees, J. Pilcher, C. Heron, P. Kiely, A comparison of clinical vs ultrasound determined synovitis in rheumatoid arthritis utilizing gray-scale, power Doppler and the intravenous microbubble contrast agent 'Sono-Vue'®, Rheumatology 46 (3) (2007) 454–459.
[17] F. Porta, G. Radunovic, V. Vlad, M.C. Micu, R. Nestorova, T. Petranova, A. Iagnocco, The role of Doppler ultrasound in rheumatic diseases, Rheumatology 51 (6) (2012) 976–982.
[18] E. Naredo, P. Collado, A. Cruz, M.J. Palop, F. Cabero, P. Richi, L. Carmona, M. Crespo, Longitudinal power Doppler ultrasonographic assessment of joint inflammatory activity in early rheumatoid arthritis: predictive value in disease activity and radiologic progression, Arthritis Care Res.: Off. J. Am. Coll. Rheumatol. 57 (1) (2007) 116–124.
[19] C.A. Scire, C. Montecucco, V. Codullo, O. Epis, M. Todoerti, R. Caporali, Ultrasonographic evaluation of joint involvement in early rheumatoid arthritis in clinical remission: power Doppler signal predicts short-term relapse, Rheumatology 48 (9) (2009) 1092–1097.
[20] A. Brown, P. Conaghan, Z. Karim, M. Quinn, K. Ikeda, C. Peterfy, E. Hensor, R. Wakefield, O. Connor, P. Emery, P: An explanation for the apparent dissociation between clinical remission and continued structural deterioration in rheumatoid arthritis, Arthritis Rheum.: Off. J. Am. Coll. Rheumatol. 58 (10) (2008) 2958–2967.
[21] M. Szkudlarek, M. Court-Payen, S. Jacobsen, M. Klarlund, H.S. Thomsen, Østergaard M: Interobserver agreement in ultrasonography of the finger and toe joints in rheumatoid arthritis, Arthritis Rheum.: Off. J. Am. Coll. Rheumatol. 48 (4) (2003) 955–962.
[22] A. Klauser, F. Frauscher, M. Schirmer, E. Halpern, L. Pallwein, M. Herold, G. Helweg, D. ZurNedden, The value of contrast-enhanced color Doppler ultrasound in the detection of vascularization of finger joints in patients with rheumatoid arthritis. Arthritis Rheum. 46 (3) (2002) 647–653.
[23] W. Schmidt, L. Volker, J. Zacher, M. Schlafke, M. Ruhnke, E. Gromnica-Ihle, Colour Doppler ultrasonography to detect pannus in knee joint synovitis, Clin. Exp. RHEUMATOLOGY 18 (4) (2000) 439–444.
[24] A.K.P. Lim, K. Satchithananda, E.A. Dick, S. Abraham, D.O. Cosgrove, Microflow imaging: New Doppler technology to detect low-grade inflammation in patients with arthritis, Eur. Radiol. 28 (3) (2018) 1046–1053.
[25] C.M. Quiñonez-Flores, S.A. González-Chávez, C. Pacheco-Tena, Hypoxia and its implications in rheumatoid arthritis, J. Biomed. Sci. 23 (1) (2016) 62.
[26] P.C. Taylor, B. Sivakumar, Hypoxia and angiogenesis in rheumatoid arthritis, Curr. Opin. Rheumatol. 17 (3) (2005) 293–298.
[27] J. Jo, G. Xu, M. Cao, A. Marquardt, S. Francis, G. Gandikota, X. Wang, A functional study of human inflammatory arthritis using photoacoustic imaging, Sci. Rep. 7 (1) (2017) 15026.
[28] K. Lund-Olesen, Oxygen tension in synovial fluids, Arthritis Rheum. 13 (6) (1970) 769–776.
[29] A.I. Richman, E.Y. Su, G. Ho, Reciprocal relationship of synovial fluid volume and oxygen tension, Arthritis Rheum. 24 (5) (1981) 701–705.
[30] M. Yang, L. Zhao, X. He, N. Su, C. Zhao, H. Tang, T. Hong, W. Li, F. Yang, L. Lin, Photoacoustic/ultrasound dual imaging of human thyroid cancers: an initial clinical study, Biomed. Opt. Express 8 (7) (2017) 3449–3457.
[31] F. Knieling, C. Neufert, A. Hartmann, J. Claussen, A. Urich, C. Egger, M. Vetter, S. Fischer, L. Pfeifer, A. Hagel, Multispectral optoacoustic tomography for assessment of Crohn's disease activity, N. Engl. J. Med. 376 (13) (2017) 1292–1294.
[32] G.L.G. Menezes, R.M. Pijnappel, C. Meeuwis, R. Bisschops, J. Veltman, P.T. Lavin, M.J. van de Vijver, R.M. Mann, Downgrading of breast masses suspicious for cancer by using optoacoustic breast imaging, Radiology 288 (2) (2018) 355–365.
[33] E.I. Neuschler, P.T. Lavin, F.L. Tucker, L.D. Barke, M.L. Bertrand, M. Böhm-Vélez, S. Destounis, B.E. Dogan, S.R. Grobmyer, J. Katzen, et al., Downgrading and Upgrading Gray-Scale Ultrasound BI-RADS Categories of Benign and Malignant Masses With Optoacoustics: A Pilot Study. *AJR*, Am. J. Roentgenol. 211 (3) (2018) 689–700.
[34] E.I. Neuschler, R. Butler, C.A. Young, L.D. Barke, M.L. Bertrand, M. Böhm-Vélez, S. Destounis, P. Donlan, S.R. Grobmyer, J. Katzen, et al., A pivotal study of optoacoustic imaging to diagnose benign and malignant breast masses: a new evaluation tool for radiologists, Radiology 287 (2) (2018) 398–412.
[35] M. Yang, C. Zhao, M. Wang, Q. Wang, R. Zhang, W. Bai, J. Liu, S. Zhang, D. Xu, S. Liu, Synovial oxygenation at photoacoustic imaging to assess rheumatoid arthritis disease activity, Radiology 306 (1) (2023) 220–228.
[36] X. Peng, A. Dentinger, S. Kewalramani, Z. Xu, S. Gray, S. Ghose, Y.T. Tan, Z. Yang, J. Jo, D. Chamberland, et al., An Automatic 3-D Ultrasound and Photoacoustic Combined Imaging System for Human Inflammatory Arthritis, IEEE Trans. Ultrason., Ferroelectr., Freq. Control 70 (12) (2023) 1691–1702.
[37] P.S. Treuhaft, D.J. McCarty, Synovial fluid pH, lactate, oxygen and carbon dioxide partial pressure in various joint diseases, Arthritis Rheum. 14 (4) (1971) 475–484.
[38] I. Steinberg, D.M. Huland, O. Vermesh, H.E. Frostig, W.S. Tummers, S.S. Gambhir, Photoacoustic clinical imaging, Photoacoustics 14 (2019) 77–98.
[39] M. Kuniyil Ajith Singh, W. Xia, Portable and affordable light source-based photoacoustic tomography, Sensors 20 (21) (2020).
[40] P.J. van den Berg, K. Daoudi, H.J. Bernelot Moens, W. Steenbergen, Feasibility of photoacoustic/ultrasound imaging of synovitis in finger joints using a point-of-care system, Photoacoustics 8 (2017).
[41] C. Zhao, Q. Wang, X. Tao, M. Wang, C. Yu, S. Liu, M. Li, X. Tian, Z. Qi, J. Li, et al., Multimodal photoacoustic/ultrasonic imaging system: a promising imaging method for the evaluation of disease activity in rheumatoid arthritis, Eur. Radiol. 31 (5) (2021) 3542–3552.
[42] G. Sakellariou, P.G. Conaghan, W. Zhang, J.W.J. Bijlsma, P. Boyesen, M. A. D'Agostino, M. Doherty, D. Fodor, M. Kloppenburg, F. Miese, et al., EULAR recommendations for the use of imaging in the clinical management of peripheral joint osteoarthritis, Ann. RHEUMATIC Dis. 76 (9) (2017) 1484–1494.
[43] M. Wang, L. Zhao, Y. Wei, J. Li, Z. Qi, N. Su, C. Zhao, R. Zhang, T. Tang, S. Liu, et al., Functional photoacoustic/ultrasound imaging for the assessment of breast intraductal lesions: preliminary clinical findings, Biomed. Opt. Express 12 (3) (2021) 1236–1246.
[44] M. Backhaus, S. Ohrndorf, H. Kellner, J. Strunk, T. Backhaus, W. Hartung, H. Sattler, K. Albrecht, J. Kaufmann, K. Becker, Evaluation of a novel 7-joint ultrasound score in daily rheumatologic practice: a pilot project. Arthritis Care Res.: Off. J. Am. Coll. Rheumatol. 61 (9) (2009) 1194–1201.
[45] T.M. Backhaus, S. Ohrndorf, H. Kellner, J. Strunk, W. Hartung, H. Sattler, C. Iking-Konert, G.R. Burmester, W.A. Schmidt, M. Backhaus, The US7 score is sensitive to change in a large cohort of patients with rheumatoid arthritis over 12 months of therapy, Ann. Rheumatic Dis. 72 (7) (2013) 1163–1169.
[46] M. Szkudlarek, E. Narvestad, M. Klarlund, M. Court-Payen, H.S. Thomsen, Østergaard M: Ultrasonography of the metatarsophalangeal joints in rheumatoid arthritis: comparison with magnetic resonance imaging, conventional radiography, and clinical examination, Arthritis Rheum.: Off. J. Am. Coll. Rheumatol. 50 (7) (2004) 2103–2112.
[47] K. McPherson, 1. Statistical methods for rates and proportions (3rd edn). Joseph L. Fleiss, Bruce Levin and Myunghee Cho Paik, Wiley, New Jersey, 2003. No. of pages: xxvii+ 760. Price: $99.95 (hardcover), ISBN: 0-471-52629-0. .: Wiley Online Libr. (2005).
[48] Hinkle D.E., Wiersma W., Jurs S.G.: Applied statistics for the behavioral sciences. (No Title) 2003.
[49] D. Ashby, Practical statistics for medical research. Douglas G. Altman, Chapman and Hall, London, 1991. No. of pages: 611. Price:£ 32.00, Stat. Med. 10 (10) (1991) 1635–1636.
[50] V. Vlad, F. Berghea, S. Libianu, A. Balanescu, V. Bojinca, C. Constantinescu, M. Abobului, D. Predeteanu, R. Ionescu, Ultrasound in rheumatoid arthritis-volar versus dorsal synovitis evaluation and scoring, BMC Musculoskelet. Disord. 12 (1) (2011) 1–9.
[51] E. Naredo, G. Bonilla, F. Gamero, J. Uson, L. Carmona, A. Laffon, Assessment of inflammatory activity in rheumatoid arthritis: a comparative study of clinical evaluation with grey scale and power Doppler ultrasonography, Ann. Rheumatic Dis. 64 (3) (2005) 375–381.

[52] U. Fearon, M. Canavan, M. Biniecka, D.J. Veale, Hypoxia, mitochondrial dysfunction and synovial invasiveness in rheumatoid arthritis, Nat. Rev. Rheumatol. 12 (7) (2016) 385–397.
[53] K. Takase-Minegishi, N. Horita, K. Kobayashi, R. Yoshimi, Y. Kirino, S. Ohno, T. Kaneko, H. Nakajima, R.J. Wakefield, P. Emery, Diagnostic test accuracy of ultrasound for synovitis in rheumatoid arthritis: systematic review and meta-analysis, Rheumatology 57 (1) (2018) 49–58.
[54] S. Ohrndorf, A.C. Boer, D.M. Boeters, R.M. Ten Brinck, G.-R. Burmester, M. C. Kortekaas, A.H.M. van der Helm-van Mil, Do musculoskeletal ultrasound and magnetic resonance imaging identify synovitis and tenosynovitis at the same joints and tendons? A comparative study in early inflammatory arthritis and clinically suspect arthralgia, Arthritis Res. Ther. 21 (1) (2019) 59.

Zhibin Huang, MD, is a resident of Ultrasound in The Second Clinical Medical College, Jinan University, China. He focuses on the clinical application of photoacoustic imaging and multi-modality imaging, especially the clinical diagnosis of diseases in breast and rheumatoid arthritics.

Sijie Mo, MD, is a resident of Ultrasound in The Second Clinical Medical College, Jinan University, China. Her fields of scientific interests: clinical application of photoacoustic imaging and multi-modality imaging, especially the clinical diagnosis of diseases in breast lesion.

Huaiyu Wu, MD, graduated from Jinan University, currently works at the Department of Ultrasound, Shenzhen People's Hospital. His research focuses on breast ultrasound, musculoskeletal ultrasound, artificial intelligence of ultrasound, photoacoustic imaging. Additionally, he has participated in a series of clinical trials in breast cancer imaging and rheumatoid arthritis imaging.

Xu Jinfeng, MD, Chief Physician, Professor of Second Clinical Medical College, Jinan University, Supervisor of Master's, Doctoral, and Postdoctoral candidates. Member of the Ultrasound Medicine Branch of the Chinese Medical Association and Deputy Leader of the Ninth Abdominal Group; Director of the Chinese Society of Ultrasound in Medicine Engineering, Deputy Chairman of the Abdominal Committee, and Deputy Chairman of the Committee on Superficial Organs and Peripheral Vessels; Vice Chairman of the Ultrasound Branch of the Guangdong Medical Association and Guangdong Medical Doctor Association; Chairman of the Ultrasound Branch of the Shenzhen Medical Association. Published more than 100 papers in national journals, over 90 papers in SCI-indexed journals, with the highest impact factor of **22.3**, and edited 5 professional books. Ranked in the top 10 national ultrasound medical scholars in 2022. Main research interests include abdominal and superficial organ ultrasound.

Fajin Dong, MD, Chief Physician of the Ultrasound Department at Shenzhen People's Hospital, Supervisor of Master's Students. Specializes in abdominal, superficial, and musculoskeletal ultrasound diagnosis and intervention therapy. Published over 60 SCI papers as the first/corresponding author (representative papers published in internationally renowned journals such as Medical Image Analysis, Research, and Nature Communications), led and participated in numerous national, provincial, and municipal projects. Serves as a committee member of the Ultrasound Branch of the Chinese Medical Association's Superficial and Vascular Group; Member of the Musculoskeletal Ultrasound Special Committee of the Chinese Medical Doctor Association & Standing Committee Member of the Interventional Physicians Branch Pain Treatment Group; Member of the Musculoskeletal Special Committee of the Chinese Society of Ultrasound in Medicine Engineering, among others.